Available online at www.sciencedirect.com
SCIENCE DIRECT®
Journal of Catalysis 220 (2003) 127–135
JOURNAL OF CATALYSIS
www.elsevier.com/locate/jcat

Characterization and photocatalytic activity of Au/TiO_2 thin films for azo-dye degradation

I.M. Arabatzis,[a] T. Stergiopoulos,[a] D. Andreeva,[b] S. Kitova,[c] S.G. Neophytides,[d] and P. Falaras [a,*]

[a] *Institute of Physical Chemistry, NCSR "Demokritos," 153 10 Aghia Paraskevi Attikis, Athens, Greece*
[b] *Institute of Catalysis, Bulgarian Academy of Sciences, "Acad. G. Bonchev" str., bl. 11, 1113 Sofia, Bulgaria*
[c] *Central Laboratory of Photoprocesses "Acad. J. Malinowski," BAS, Acad. G. Bonchev str., bl.109, Sofia 1113, Bulgaria*
[d] *FORTH-ICE/HT, PO Box 1414, 26500 Patras, Greece*

Received 19 February 2003; revised 15 May 2003; accepted 15 May 2003

Abstract

Surface modification of rough, high-surface area, nanocrystalline titania thin-film photocatalysts was performed by gold deposition via electron beam evaporation, with an attempt to enhance the decomposition reaction rate of industrial water pollutants. The materials were characterized and their photocatalytic activity was tested for methyl orange photodegradation. The surface deposition of gold particles improves the photocatalytic efficiency of the titania films by the synergetic action on the charge separation process onto the semiconductor. The most advantageous surface concentration of gold particles in the composite Au/TiO_2 photocatalyst was found to be 0.8 μg cm^{-2}, leading to a two times faster degradation of methyl orange with respect to the rate obtained with the original TiO_2 material. Higher surface loadings result in an efficiency decrease, and this can be understood in terms of an optimum gold particle size and surface characteristics as well as the semiconductor availability for light absorption and pollutant adsorption. No deactivation of the catalyst was observed after five consecutive photocatalytic experiments of new added pollutant.

Keywords: TiO_2 nanocrystalline thin films; Doctor-blade technique; Gold deposition; Photocatalyst activity; Azo-dyes; Methyl orange; Pollutant degradation

1. Introduction

Heterogeneous photocatalysis based on TiO_2 is one of the most active and the most promising advanced oxidation processes (AOPs), as this semiconductor is a low-cost, nontoxic, and stable material. It has been the focal point of numerous investigations in recent years particularly because of its application on the quantitative destruction of undesirable chemical contaminants [1–3]. The applicability of the process depends on its operating cost and efficiency. In the case of aqueous powder dispersions, one significant drawback is the cost of separating TiO_2 from the water after treatment, by either sedimentation and/or ultrafiltration. To overcome this obstacle, recent investigations on TiO_2 photocatalysis are oriented toward the photocatalyst immobilization in the form of thin films [4,5]. The photocatalyst immobilization/stabilization technique eliminates the majority of the problems encountered with slurries (particle aggregation, need for filtration) and enables the development of self-cleaning and self-sterilizing surfaces [6].

Gold, dispersed as ultrafine particles and supported on metal oxides, exhibits an extraordinary high activity for low-temperature catalytic combustion, partial oxidation of hydrocarbons, hydrogenation of unsaturated hydrocarbons, and reduction of nitrogen oxides [7–13]. A series of titania–metal composite nanoparticles (mainly noble metals and noble/transition metal ions) have been used in order to increase the efficiency of the photocatalytic process [14–16]. Dawson and Kamat [17], by a laser flash photolysis study, proved that there is an enhancement in the hole transfer of gold-capped TiO_2 nanoparticles; however, the authors obtained only a 10–15% increase in photocatalytic efficiency in the case of the corresponding thin films [8] and raised the question as to what extent do gold nanoparticles improve the photocatalytic activity of TiO_2 films. Recent investigations on gold titania nanocomposite particles show that metal ion doping extended the response of the photocatalyst into the visible; however, a significant decrease in

* Corresponding author.
E-mail address: papi@chem.demokritos.gr (P. Falaras).

0021-9517/$ – see front matter
doi:10.1016/S0021-9517(03)00241-0

their photocatalytic performance under UV illumination [18] was observed. Looking for a plausible explanation, some authors raised the question of the identity of the gold species (metal/metal ion), which might have an influence on the activity of the titania/gold photocatalyst [19]. It is now well established that the catalytic properties of Au depend on the support, the preparation method, and particularly the shape and size of the Au clusters [20]. On the other hand, it must be pointed out that most of the literature on TiO_2 photocatalysis are focused on the photocatalytic gold/titania colloids and only a few number deal with thin film surfaces [18,21–27]. It is therefore a necessity to further explore and understand the behavior of the gold-modified titania thin-film photocatalysts.

This work aims to develop new composite immobilized photocatalysts of increased efficiency, consisting of gold particles deposited on rough high-surface-area nanocrystalline TiO_2 thin films based on commercially available Degussa P-25. Our intension is to modify the titania photocatalysts in order to produce immobilized systems for further exploitation in continuous flow reactors. The new, modified catalyst is characterized by means of spectroscopy and microscopy in order to elucidate the gold valence state, structure, and morphology. Effects of metal loading on the UV-light photocatalytic activity are presented and discussed in terms of surface morphology. The gold-modified nanocrystalline titania thin-film photocatalyst has been tested to compare its photocatalytic efficiency to that of the nonmodified material. Subsequently, to evaluate the catalytic activity, the photodegradation of a well-known organic azo-dye methyl orange (MO) is investigated as a simple model compound, under near-UV irradiation.

2. Experimental

The pollutant used in this work was methyl orange ([4-[[(4-dimethylamino)phenyl]-azo]benzenesulfonic acid sodium salt] with the molecular formula $[(CH_3)_2NC_6H_4N{=}NC_6H_4SO_3Na]$) or acid orange 52. MO is very stable and can be considered a typical azo-dye in the textile industry. The pollutant and all reagents utilized for the synthesis of the photocatalysts were of analytical grade from Fluka (Switzerland). Ultrapure water was obtained from a USF Purelab plus (Germany) apparatus. O_2 stream was of 99.999% purity.

Rough, high-surface-area nanocrystalline TiO_2 thin films were prepared on microscopy glass slides applying the doctor-blade procedure and used as the photocatalyst substrates [27]. In order to visualize only the gold particles, smooth and well-ordered nanostructured TiO_2 films were also fabricated by applying a combination of sol-gel and spin-coating techniques [27,28]. Gold films were deposited by electron beam evaporation of a Au wire (ultrahigh purity), under vacuum better than 6×10^{-4} Pa, onto stationery, titania-coated microscopical slides, placed in parallel to the emitting surface. Quartz crystal monitor was used for controlling the deposition rate of 0.01 $\mu g\,cm^{-2}\,s^{-1}$. By varying the deposition time, various amounts of gold were deposited: 0.4, 0.8, 1.6, and 2.0 $\mu g\,cm^{-2}$. The amount of Au, condensed at each point of the substrate was calculated from the crystal monitor data, by applying the method described in Ref. [29].

UV–vis diffuse reflectance spectra were obtained with a Hitachi U-4001 spectrophotometer equipped with an integrating sphere. To elucidate the gold valence state, X-ray photoelectron spectroscopy (XPS) experiments were carried out in an ultrahigh vacuum chamber equipped with a hemispherical electron analyzer (SPECS LH-10) and a twin-anode X-ray source, using the unmonochromatized Mg-K_α at 1253.6 eV and an analyzer pass energy of 97 eV. The structural properties of the photocatalysts were analyzed with an X-ray diffractometer (Siemens D-500, Cu-K_α radiation). To compare and complete the XPS results, Raman spectroscopy (LABRAM from JOBIN-YVON spectrometer equipped with a microscope, CCD detection, and a 514.5 nm Argon laser line) was employed. Detailed surface images were obtained by means of a scanning electron microscope (SEM) with numerical image acquisition (LEICA S440). Carbon deposition has been performed to avoid problems arising from surface charge effects. X-ray from the SEM microscope probe (at horizontal incidence beam) was used for the nondestructive qualitative and quantitative chemical analysis of the modified films. Surface morphology, roughness, and fractality of the gold/titania films were examined with a Digital Instruments Nanoscope III atomic force microscope (AFM), operating in the tapping mode (TM) [27,30].

To evaluate the catalytic activity of the gold/TiO_2 films, photocatalysis experiments were carried out or round-bottomed photocatalytic Pyrex glass cells (cutoff wavelength: 320 nm) and methyl orange was the model pollutant for destruction. The irradiation system is equipped with four parallel F15W/T8 blacklight tubes (Sylvania GTE), which have maximum emission at 350 nm. The irradiance of the system was measured using an 28-0925 Ealing Research Radiometer-Photometer operating in conjunction with a 28-0982 silicon detector and a 28-0727 flat response filter and has been found to be of 71.7 $\mu W\,cm^{-2}$. Aqueous solutions of methyl orange (4 ml) were photolyzed in the presence of modified TiO_2 thin films (accurately cut in surface areas of 0.8 cm^2) under magnetic stirring. All solutions were O_2-bubbled for 2 h prior to use in order to achieve dissolved oxygen saturation. Initial pollutant concentration was set to 2.056×10^{-5} M. Spectrophotometrical analytical determination was carried out at 466.5 nm ($\varepsilon_{MO} = 25{,}100\ M^{-1}\,cm^{-1}$).

3. Results and discussion

For the preparation of the nanocrystalline titania thin films, the doctor-blade technique can be easily employed as a fast and nonenergy-consuming procedure for mass production, with good uniformity and reproducible properties [31].

After gold deposition, the photocatalyst color appears purple. Increasing the Au deposition time produces thicker and darker films at a gradient rate. Observation of the film with an optical microscope suggests that gold particles are widely spread on the surface without the formation of islands. The resulting surface-modified photocatalysts possess a solid structure on the glass substrate with a satisfactory scratch resistance and adherence. This is attributed to the titania substrate deposition method.

Fig. 1 illustrates the visible (i) and near-UV (ii) reflectance spectra of untreated doctor blade (Degussa P25 TiO_2) and the corresponding Au/TiO_2-modified thin films. The addition of gold induces significant changes to the spectrum of TiO_2 films: a gradient decrease of the reflectance around 545 nm is attributed to the surface plasmon resonance and indicates enhanced visible photon capture at the visible region. This absorption is ascribed to a collective oscillation of the free conduction band electrons of the gold particles in response to optical excitation [32,33]. The band is strongly dependent on the shape and the size of the gold clusters [34], becomes broad for cluster sizes greater of 50 nm (see microscopy characterization section) and tends to cover the visible region (Fig. 1i). It must also be pointed out that gold deposition results in an important shift of the absorption edge to higher wavelengths (Fig. 1ii). Such an absorption edge red shift for the gold modified titania materials depends directly on the Au load.

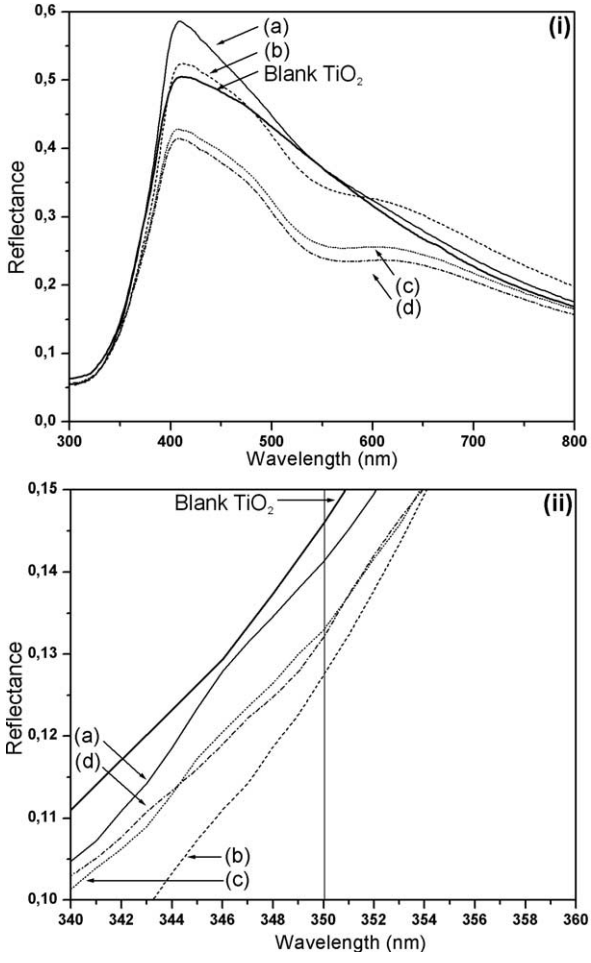

Fig. 1. Reflectance spectra of an untreated Degussa P25 TiO_2 film and of composite Au/TiO_2 films with Au surface loads of 0.4 $\mu g\,cm^{-2}$ (a), 0.8 $\mu g\,cm^{-2}$ (b), 1.6 $\mu g\,cm^{-2}$ (c), and 2.0 $\mu g\,cm^{-2}$ (d). Upper diagram (i) represents the wide range spectra while the lower one (ii) zooms in the irradiation region (350 nm).

To elucidate both the chemical oxidation state of the gold particles and the nature of titanium species, X-ray photoelectron spectroscopy (XPS) experiments were performed. The binding energy of the Ti(2p) electrons was 459.5 eV, leaving no doubt for the extensive existence of $Ti^{IV}O_2$. Fig. 2 shows the XP spectra of the Au(4f) electrons for various quantities of gold, which have been deposited on thin films of TiO_2. Au coverages as determined by XPS measurements vary between 0.04 monolayers and 0.15 monolayers (Table 1). The quantitative analysis was based on layer formation of Au on

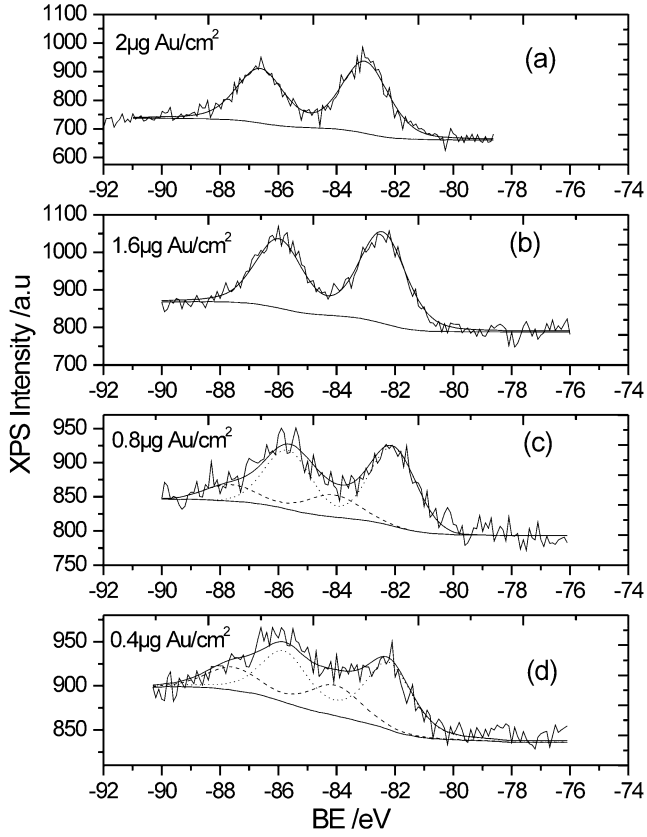

Fig. 2. Au(4f) XPS spectra for the gold/titania films. (a) 2.0 $\mu g\,cm^{-2}$ Au/TiO_2, (b) 1.6 $\mu g\,cm^{-2}$ Au/TiO_2, (c) 0.8 $\mu g\,cm^{-2}$ Au/TiO_2, and (d) 0.4 $\mu g\,cm^{-2}$ Au/TiO_2.

Table 1
Metal surface coverage as determined from XPS results

($\mu g\,cm^{-2}$ Au on TiO_2)	0.4	0.8	1.6	2.0
Surface coverage Φ_A	0.037	0.066	0.139	0.147
Au surface area (cm^2)	14.8	26.4	55.6	58.8

The gold surface area (in cm^2) corresponding to film samples of 0.8 cm^2 in geometric area (of 400 cm^2 in real surface extension) is also given.

TiO_2 according to the equations [35]

$$I_B = I_B^{\infty}\left[1 - \Phi_A + \Phi_A \exp\left(-d_A/\lambda_A^{(E_B)}\cos\theta\right)\right], \quad (1)$$

$$I_A = I_A^{\infty}\Phi_A\left[1 - \exp\left(-d_A/\lambda_A^{(E_B)}\cos\theta\right)\right], \quad (2)$$

where $\lambda_{AB}^{E_A}$ and $\lambda_{AB}^{E_B}$ are the mean free paths of the photoelectrons with kinetic energies E_A and E_B in the solid composed of the mixture of A and B. I_A^{∞} and I_B^{∞} are the intensities of clean A and B materials. Φ_A is the coverage of the deposited material A. The ratio $I_A^{\infty}/I_B^{\infty}$ is constant for $\theta = 0$. Using the gold coverage, as determined by the XPS measurements, and taking into account that the roughness factor (real surface area to geometric surface area ratio) of a doctor blade titania film is about 500 [36], the Au surface area was estimated for the different Au/TiO_2 catalysts (samples of 0.8 cm^2 in geometric surface area and 400 cm^2 in real surface extension) and the results have been incorporated in Table 1.

The binding energy of the Au(4f) spectra was corrected with respect to the binding energy of Ti(2p3/2) photoelectrons, which was considered at 495.5 eV for the TiO_2 [35]. The shift toward lower binding energies as compared to metallic Au can be due to the negative charging of the Au nanoparticles because of the charge transfer from the TiO_2 substrate. The negative charging of the Au nanoparticles can be understood because of the large difference in the work-function of Au (5.42 eV) and TiO_2 (4.7 eV); thus, electron transfer is facilitated from lower (TiO_2) to higher (Au) work-function [37]. The phenomenon as expected is more intense for lower Au loadings most probably due to the smaller particle size.

The deconvoluted Au(4f) peaks (Figs. 2c and 2d) at low Au loadings (0.4 and 0.8 $\mu g\,cm^{-2}$) show that Au nanoparticles are partially oxidized. The peak at 82.15 ± 0.1 eV is attributed to metallic Au while the peak at 84.05 ± 0.1 eV is situated 1.9 eV toward higher binding energy and corresponds either to the oxide (Au_2O_3) or oxyhydroxide (AuOOH) chemical state of Au particles [37]. This behavior can be due to the spillover of O^{2-} or OH^- from the TiO_2 support all over the gold particles [38]. Subramanian et al. [18] working on gold-capped TiO_2 nanocomposite particles postulate that photogenerated holes ($E_{vb} \sim 2.5$ V SCE are capable of oxidizing noble metals [e.g., $E^0(Au/Au^+) = 1.76$ V] present at the interface. Although most of the photogenerated holes are scavenged by the surface hydroxyl groups, a small fraction of these holes may participate in the oxidation of Au^0 at the TiO_2 interface [19]. It is worth noting that at the lowest Au loading (Fig. 2d) where the particle size is smallest the detected amount of the oxidation state of Au is highest, indicating the effect of the particle size on the oxygen or hydroxide affinity of Au particles.

The X-ray diffraction profiles (not shown) suggest that the gold particles are not crystallized on TiO_2 surfaces. After prolonged deposition time (Au load of 2.0 $\mu g\,cm^{-2}$), a very weak peak at $2\theta = 44.14°$ is observed, revealing the presence of a metallic gold phase [39]. A more intense peak was expected at 38.2° for Au^0, nevertheless titanium dioxide XRD pattern overlaps this reflection. On the contrary, a well-organized crystal structure from titania particles is observed for the films. The anatase reflections dominate in the reflection patterns but rutile is also present [40], as the original material (TiO_2 Degussa P25) contains both phases ($\sim 75\%$ anatase and $\sim 25\%$ rutile). The strongest peak at $2\theta = 25.2°$ is representative for (101) anatase phase reflections, where by applying the Scherrer formula, the TiO_2 crystallites size can be estimated at 23 nm.

Table 2
X-ray analysis (SEM) on gold-modified TiO_2 samples

Sample	Typical Au load	Wt%		At.%	
		Ti-L	Au-M	Ti-L	Au-M
Au Degussa P25 TiO_2	0.4 $\mu g\,cm^{-2}$	89.99	1.72	85.19	0.40
Au Degussa P25 TiO_2	0.8 $\mu g\,cm^{-2}$	90.28	4.61	89.38	1.11
Au Degussa P25 TiO_2	1.6 $\mu g\,cm^{-2}$	90.36	7.89	94.74	2.01
Au Degussa P25 TiO_2	2.0 $\mu g\,cm^{-2}$	83.53	13.67	90.69	3.61
Au Sol-gel TiO_2	0.4 $\mu g\,cm^{-2}$	26.94	1.17	13.06	0.12
Au Sol-gel TiO_2	0.8 $\mu g\,cm^{-2}$	25.99	2.93	11.33	0.31
Au Sol-gel TiO_2	1.6 $\mu g\,cm^{-2}$	24.93	12.06	12.20	1.43
Au Sol-gel TiO_2	2.0 $\mu g\,cm^{-2}$	26.25	11.69	12.85	1.39

To estimate the Au/Ti atomic concentration ratio on the surface of Au/TiO_2 films, X-ray chemical analysis (by using a SEM microscope) was performed on 5×5-mm surfaces. The results (Table 2) clearly show that by increasing the deposition time solution, the corresponding gold weight percentage increases. An increased gold to titanium ratio (Au/Ti) for the sol-gel films is observed, which is attributed to the lower TiO_2 content of the corresponding films. Actually, these films are very thin compared to the doctor-blade-manufactured films and possess a flat surface (see Microscopy). In general, similar results to the Au content increase trend were observed on both the Doctor-blade and sol-gel films, thus confirming our hypothesis that the choice of the titania substrate does not affect the gold deposition process.

Raman spectroscopy was applied to unambiguously discriminate the local order characteristics of the films. The technique (nondestructive) is capable of elucidating the photocatalyst structural complexity as peaks from each material are clearly separated in frequency, and therefore the phases are easily distinguishable. Laser power output was set to 1 and 10 mW. The Raman spectra with the assigned vibration modes [41] for the TiO_2 samples at both laser intensities are shown in Fig. 3. A well-resolved TiO_2 Raman peak is observed at 145 ± 2 cm^{-1} for all the films examined. This peak is attributed to the main E_g anatase vibration mode. Furthermore, vibration peaks at 195 ± 3 cm^{-1} (E_g, weak), 397 ± 1 cm^{-1} (B_{1g}), 517 ± 2 cm^{-1} (A_{1g}), and 638 ± 2 cm^{-1} (E_g) are present in the spectra of all samples, indicating that for the substrate, anatase nanoparticles are the predominant species. However, the rutile phase is observed as a broad peak at 448 ± 1 cm^{-1}, originating from the mixed-phase original material (Degussa P25 TiO_2). The relative intensity

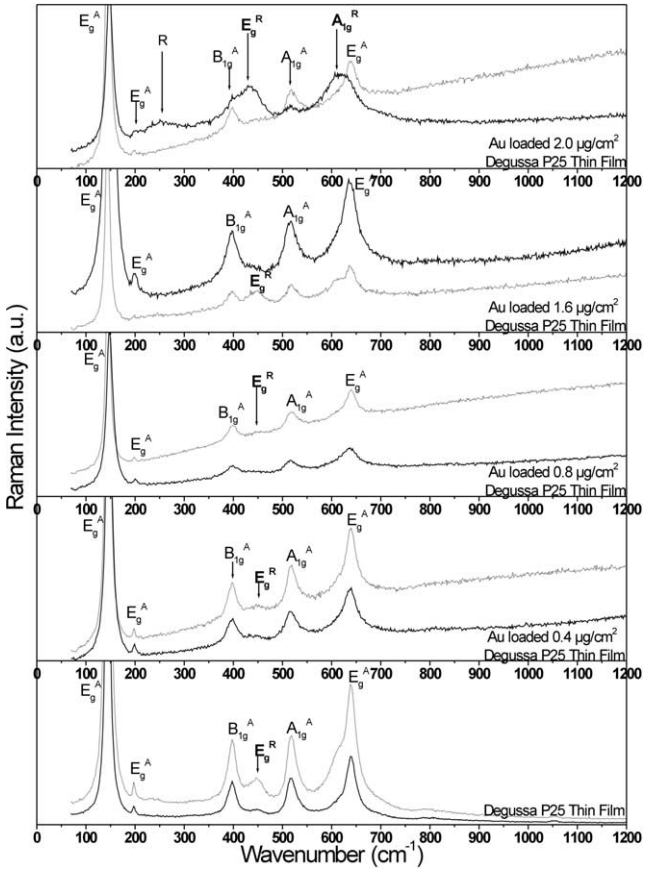

Fig. 3. Raman spectra of gold-modified doctor-blade Degussa P25 TiO_2 film. Dotted lines represent 1 mW laser output; solid lines represent 10 mW.

of the Raman bands was modified upon prolonged gold deposition and strong laser irradiation. The most characteristic example is the spectrum of the 2.0 $\mu g\,cm^{-2}$ Au/TiO_2 thin film where the intensity of the rutile peaks at 438 cm^{-1} (E_g) and 621 cm^{-1} (A_{1g}) increase dramatically. A broad band at 254 cm^{-1} is assigned as disorder or second-order scattering of the rutile phase [42]. As a consequence, it is assumed that rutile phase content increases after laser irradiation in presence of Au. This phenomenon is most obvious by increasing the laser output. It is known that transition metal impurities catalyze phase transformation of TiO_2 upon heating [43]. To the best of our knowledge, anatase-to-rutile phase transformation is not reported under laser irradiation and/or heating in the presence of gold particles. This observation is currently under examination.

An important point raised by recent works on the subject is to what extent do gold particles improve the photocatalytic activity of TiO_2 films. To evaluate the UV photocatalytic activity of $OTE/TiO_2/Au$ film electrodes toward acid orange 7, Kamat and co-workers [8] used the decrease in the dye absorbance band at 480 nm, reflecting the disappearance of the dye. The increase in the degradation rate with $OTE/TiO_2/Au$ was only about 10–15% greater than the one obtained with OTE/TiO_2 film. In our case, the film's activity was evaluated through photocatalysis experiments that took place in aqueous solutions of methyl orange. The pollutant solution was first photolyzed in the absence of photocatalyst to examine its stability. In that case, the experimental results verify that the azo-dye is not decomposed even after long-time irradiation. The photocatalytic activity was then expressed as the percentage pollutant disappearance. Each experimental set was repeated three times. The results were reproducible within narrow limits ($\leqslant 4\%$) and the mean value was selected.

Preliminary tests confirmed that the crucial parameter that strongly influences the films photocatalytic activity is the amount of the deposited gold (surface load). The results show that by gold deposition on the titania substrate, the photocatalytic efficiency increases. In Table 3, the decomposition percentage for the MO solution's decolorization corresponding to 1 h illumination, in the presence of the gold-modified titania films, is reported. The corresponding performance of the original nonsupported doctor-blade titania films is also given for comparison. A maximum (72%) is observed for the titania films modified with 0.8 $\mu g\,cm^{-2}$ gold, which is twice the corresponding MO degradation percentage obtained with pure titania. Further increase of the Au load results in a considerable efficiency decrease; however, it is important to note that the efficiency of the gold-modified materials remains always higher than the nonmodified catalysts. The above behavior is in excellent agreement with the reflectance spectra (Fig. 1) and can be roughly explained by the amount of absorbed photons. In fact, the absorbance values of the film photocatalysts follow the same tendency with the photocatalytic efficiency, in the region of the lamp emission spectrum.

Fig. 4 presents the MO photodegradation kinetics and permits a direct comparison of the performance of the gold-modified photocatalyst to the nonsupported material. Under the experimental conditions used, the photocatalytic curves follow first-order reaction kinetics. It is well es-

Table 3
Kinetic parameters and photocatalytic efficiency (%) of the titania films toward MO photodegradation

	TiO_2	Au/TiO_2 0.4 $\mu g\,cm^{-2}$	Au/TiO_2 0.8 $\mu g\,cm^{-2}$	Au/TiO_2 1.6 $\mu g\,cm^{-2}$	Au/TiO_2 2.0 $\mu g\,cm^{-2}$
MO degradation (%) (after 1 h illumination)	34.95	53.41	72.11	55.45	49.34
Time to complete decolorization (h)	5.5	3.5	2.5	3.2	4.1
Decomposition rate constants (min^{-1})	0.0103	0.0157	0.0241	0.0191	0.0150
Photonic efficiency (Φ_λ)*	0.084	0.128	0.197	0.156	0.123

* Determined as the ratio of the number of molecules converted to the number of incident photons, at $\lambda = 350$ nm.

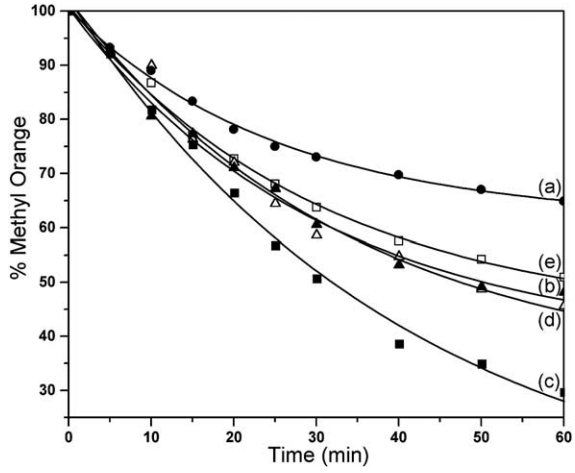

Fig. 4. Decomposition kinetics of MO (4 ml of 1.9×10^{-5} M, initial pH 9.2) in the presence of a Degussa P25 TiO_2 film (●, a), Au/TiO_2 0.4 μg cm^{-2} (▲, b), Au/TiO_2 0.8 μg cm^{-2} (■, c), Au/TiO_2 1.6 μg cm^{-2} (△, d), Au/TiO_2 2.0 μg cm^{-2} (□, e) photocatalysts.

tablished [44] that photocatalysis experiments follow the Langmuir–Hinshelwood model, where the reaction rate R is proportional to the surface coverage θ,

$$R = -\mathrm{d}C/\mathrm{d}t = k_\mathrm{r}\theta = k_\mathrm{r}KC/(1+KC), \tag{3}$$

where k_r is the reaction rate constant, K is the adsorption coefficient of the reactant, and C is the reactant concentration. When C is very small, the KC product is negligible with respect to unity so that Eq. (3) describes a first-order kinetics. The integration of Eq. (3) with the limit condition that at the start of irradiation, $t = 0$, the concentration is the initial one, $C = C_0$, gives

$$-\ln(C/C_0) = k't, \tag{4}$$

where k' is the apparent first-order reaction constant. Kinetic parameters resulting from the application of Eq. (4), percentage of degradation after 1 h of illumination and time for complete decolorization are summarized in Table 3. It is obvious that the gold-modified materials are more efficient photocatalysts compared to the pure titania Degussa P25 film, presenting higher degradation percentages and rate constants for the decomposition of MO. In fact, in the absence of gold deposition, titania films decompose MO with a rate constant of 0.0103 min^{-1}. At low concentrations of gold we observe an increase in the efficiency of the photooxidation process. For a gold surface loading of 0.8 μg cm^{-2}, we obtained an enhancement of 230% in the reaction rate constant. By further increasing the gold concentration, the reaction rate decreases and this can be attributed to the inability of the photogenerated holes to reach the interface as well as to an increased absorption of the gold [24]. Complete pollutant decolorization was also faster and was achieved after 2.5 h of illumination in the case of the 0.8 μg cm^{-2} Au/TiO_2 material, while for the titania film the process took more than 5 h.

Rough, high-surface-area nanocrystalline titania films show an amazing ability to efficiently capture photons, throughout a thick semiconducting network acting in a "sponge"-like way [16]. One must take also into account that in the case of a heterogeneous photocatalytic process with a TiO_2 thin film catalyst, adsorption on the photocatalyst typically takes place. The apparent increase in photocatalytic activity of the modified Au/TiO_2 films in comparison with TiO_2 may be due to their unique textural characteristics. As a matter of fact, in such a composite material, photocatalysis is not a simple surface process. The resulting catalyst presents a composite surface which functions both as photons capturing sponge and as gold-promoted substrate. The surface coverage and the diameter of the nanoparticles are essential parameters to take into account [45] and it is well established that small metal islands deposited on the TiO_2 surface provide a favorable geometry for facilitating the interfacial charge transfer under UV irradiation [24].

The photocatalytic behavior can be explained on the basis of surface characteristics. It is well known that the gold synergetic effect in a catalytic procedure is closely related to the size and shape of the surface particles [20]. To better understand the differences between the Au/TiO_2 films and express this in terms of surface parameters, we have undertaken the characterization of their texture and morphology, by both scanning electron microscopy and atomic force microscopy. The SEM image (not shown) confirms that the doctor-blade titania substrate presents a porous, sponge-like network of high roughness and complexity which results in a high-surface-area titania film, extremely efficient for the photodegradation of organic compounds [16]. On such high roughness titanium dioxide morphology, it is impossible to visualize the gold particles (we note that SEM X-ray analysis and XPS measurements confirmed the presence of gold onto the titania substrate). Despite the importance of the surface roughness for the efficiency of the photocatalytic process, the existence of an irregular and porous TiO_2 substrate makes a "natural screening" and creates an insurmountable problem to the gold particles imaging.

In order to overcome the above problem, the gold deposition procedure was performed on very thin ($\sim$ 300 nm in thickness) and flat titanium dioxide films prepared via a sol-gel technique [16]. On relatively smooth modified surfaces, the use of SEM and AFM permitted a direct observation of the gold particles. It is important to note that the gold particles are well distributed over the titania sol-gel films in the examined concentration range (Fig. 5). Their surface density (number of particles per surface unit) and average grain diameter depends on the gold deposition time. Increasing the deposition time of gold results in an enhancement over the particle's diameter. This is better and directly illustrated in Fig. 6, which shows the corresponding AFM 5×5-μm^2 surface plots (three-dimensional representations). The relevant surface parameters such as grain diameter, roughness, fractal dimension, and height of surface features [16,46–48] are reported on Table 4. Once again, we can confirm that the

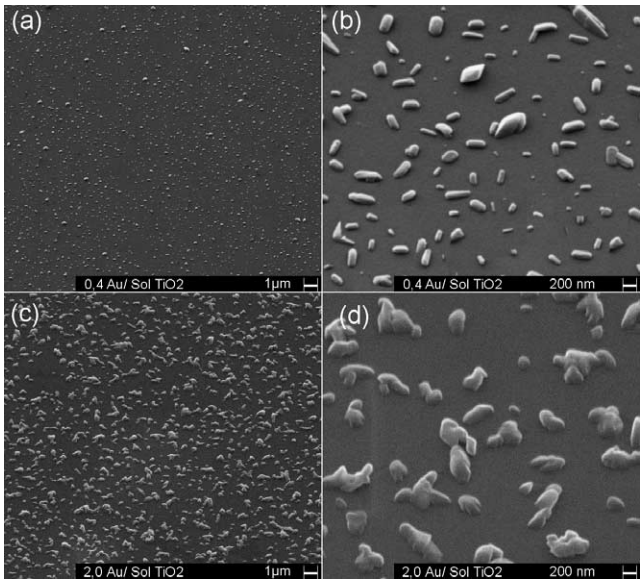

Fig. 5. SEM pictures of gold-modified sol-gel TiO_2 films: Au/TiO_2 0.4 μg cm^{-2} (a, b), Au/TiO_2 2.0 μg cm^{-2} (c, d).

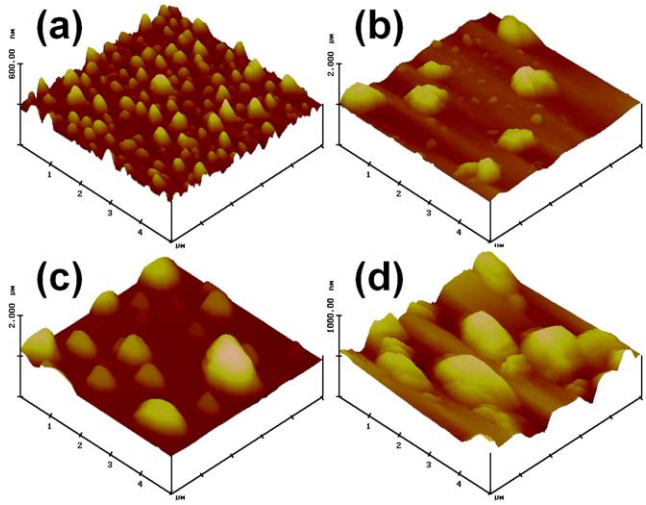

Fig. 6. 3D AFM surface plots for gold/titania sol-gel films: Au/TiO_2 0.4 μg cm^{-2} (a), Au/TiO_2 0.8 μg cm^{-2} (b), Au/TiO_2 1.6 μg cm^{-2} (c), Au/TiO_2 2.0 μg cm^{-2} (d). Note the difference on the z range of the Au/TiO_2 0.4 μg cm^{-2} film.

size and frequency of metal particles over the semiconductor surface strongly depend on the preparation conditions and especially on the gold deposition time and finally the Au load. In fact, it is important to note that the values of the majority of the surface parameters present a standard increase, by extending the gold coverage on the titania surface. The "irregular" behavior of the fractal dimension can be attributed to the existence of two different groups of gold features. A network of well-distributed small particles exists underneath a group of distinct larger "rock" aggregates (Fig. 6b). The coexistence of gold particles of both small and large size is at the origin of the observed enhancement in the photodecomposition of MO reaction rate constant. It can be easily understood that the complexity and feature's frequency of such a surface is not expected to be extremely high but on the contrary, this is consistent with a low fractal dimension value. However, it is important to note that this material (0.8 μg cm^{-2}) presents the highest photocatalytic activity. By increasing the gold surface loading, the size of gold particles significantly increases and this seriously affects (decreases) the photocatalytic reaction rate.

In heterogeneous photocatalysis, the photonic efficiency, Φ_λ, can be used to describe the number of molecules converted relative to the total number of photon incidents on the reactor. This corresponds to the so-called "apparent" or lower limits of the actual quantum yield and it is based on the assumption that all the incident photons are absorbed by the photocatalyst (the solid photocatalyst surface in our case). By taking into account the decomposition rate constants, a pollutant initial concentration of 2.056×10^{-5} M and a light irradiance of 71.7 μW cm^{-2}, the corresponding photonic efficiency values, Φ_λ, were calculated at $\lambda = 350$ nm and reported in Table 3. However, it must be taken into account that the above calculated Φ_λ values are not stadardized, as the number of absorbed photons is experimentally difficult to access.

Catalysts are in general metastable materials. This means that in time their properties change, often accompanied by deactivation. The deposition of a noble metal on semiconductor nanoparticles is in general beneficial for maximizing the efficiency of photocatalytic reactions. However, any deterioration of the metal of the metal/semiconductor interface during the long-term operation of the photocatalyst is likely to limit the benefits of metal deposition. Over the long-term UV irradiation, semiconductor metal composite films exhibit a decrease in photocatalytic performance [19]. The observed deterioration of the catalytic property has been attributed to the possibility of oxidation of the metal by the photogener-

Table 4
Average grain diameter, roughness, fractal dimension, and surface parameters for gold deposition on TiO_2 films (from AFM analysis)

Typical Au surface concentration	0.4 μg cm^{-2}	0.8 μg cm^{-2}	1.6 μg cm^{-2}	2.0 μg cm^{-2}
Average particle diameter (nm)	50	76	740	1120
Roughness Rms (nm)	29.9	72.94	113.93	120.38
Fractal dimension (D_f)	2.37	2.15	2.39	2.34
Max of height distribution (nm)	38.2	148.16	157.2	194.5

Rms, the standard deviation of the z values, z being the total height range analyzed. Fractal dimension D_f ($3 \geqslant D_f \geqslant 2$), parameter which accounts for the geometric surface complexity and reflects the scaling behavior. It has been calculated by using the V423r3 algorithm [16,46–48].

ated holes and/or surface hydroxyl radicals. The oxidation of gold by the photogenerated holes and reduction of gold ions by conduction band electrons compete to decide the ultimate fate of the interface. In our case, no noticeable differences were observed in the UV–vis absorption spectra of the photocatalysts before and after the photocatalytic experiments. This excludes the possibility of further transformation of the Au/TiO_2 interface (oxidation of Au intercalation of Au^+ into TiO_2), during photocatalysis.

The strength and reproducibility of the photocatalytic activity on the gold-supported TiO_2 doctor-blade films were examined in order to check their potential use in practical systems. Thus, the immobilized Au/TiO_2 film surface (0.8 $\mu g\,cm^2$) was used in five consecutive irradiation experiments—cycles of new added pollutant substrate quantities (the same photocatalyst with renewed pollutant solution). The photocatalyst was very stable and did not loose activity with repeated uses, as the decomposition kinetics of MO did not show any dependence on the cycle number. Each experiment included 1 h of illumination and reproduced well the initial results (reaction rate constant and decomposition percentage of MO pollutant) within 2–4%. On the other hand, it must be pointed out that no loss of activity of the photocatalyst was observed during storage for several days in the dark, both under argon atmosphere and in MO solution. The obtained results make further research on the subject very encouraging. This work opens the possibility of developing more efficient composite photocatalysts in the form of porous and high-surface-area inorganic oxide matrices doped with different other metal additives (i.e., Ru, Ag). In this direction, the use of TiO_2 precursors with long-range particle-size distribution may produce films with high surface development and increased efficiency in light harvesting.

On the basis of the activity measurements and structural characterization of the photocatalysts, a reaction mechanism involving the participation of the gold metal particles is proposed. Illumination of the TiO_2 films by photons of energy greater than the band gap energy ($E_g = 3.2$ eV) creates pairs of electrons (e^-) and holes (h^+) following the reaction:

$$TiO_2 + h\nu \rightarrow TiO_2\ (e^-, h^+). \tag{5}$$

In the valence band, the photogenerated holes migrate to the interface and react with OH^- adsorbed onto the TiO_2 to create hydroxyl radicals (·OH):

$$(TiO_2)\ldots OH^- + h^+ \rightarrow \cdot OH. \tag{6}$$

In the conduction band the photoinduced electrons react with electron acceptors such as oxygen-creating oxygen radicals ($O_2\cdot^-$) [46,47]. These radicals (·OH, $O_2\cdot^-$) present extremely strong oxidizing properties and are able to decompose the MO pollutant through a reaction involving several sulfonated intermediates together with the formation of the inorganic final products (SO_4^{2-}, NO_3^-, NH_4^+) [49], carbon dioxide and water:

$$\cdot OH/O_2\cdot^- + MO \rightarrow (\text{sulfonated intermediates}) \rightarrow SO_4^{2-} + NO_3^- + NH_4^+ + CO_2 + H_2O. \tag{7}$$

In the case of the gold/titania composite photocatalysts, it has recently been shown that both the presence of Au(III) and Au^0 species at the TiO_2 interface is beneficial for the photocatalytic process at low concentration levels (higher loadings have a negative effect) [18]. The observed enhancement has been attributed to two distinct mechanisms: to the electron scavenging by Au(III) ions which suppresses the charge recombination process, and to the interfacial charge transfer at the semiconductor interface promoted by the metal (Au^0) particles. A number of the conduction band electrons can be attracted by the metal particles due to the difference in the work function between gold and titania. Li and Li [11] proposed that the presence of Au(0) on TiO_2 surfaces favors the migration of photoproduced electron to gold, thus improving the electron/hole separation. On the other hand, one could assume that the metal-semiconductor contact is not ohmic but has a Schottky barrier character. As a result, electrons excited by illumination move to the metal surface through the conduction band, driven by an electric field, and the light-induced charge separation becomes easier [50]. Such an efficient electron "capture" improves the charge separation process and avoids electron-hole pair recombination. Consequently, the photocatalytic efficiency increases [51]. The above mechanism is consistent with the highest photocatalytic activity observed for the gold-modified films with respect to nonsupported titania. It is also compatible with the relative increase in the photocatalytic efficiency observed for the composite catalysts corresponding to low gold contents and justifies the relative activity decrease observed in the case of gold loadings higher than an optimum value. In fact, it is well understood that as the gold particles aggregate and their diameter increases, the photoinduced electrons attracted by the gold particles are not in close proximity of the holes and can therefore be efficiently separated. However, one must have in mind that the heterogeneous photocatalysis is a surface process and the gold-supported catalysts have different surface characteristics. This results in differences in the total titania surface area exposed to the light beam and that available for pollutant adsorption. An antagonism between the gold synergetic action following the mechanism described above and a natural screening resulting from the presence of gold excess on the titania surface cannot be excluded. The optimum gold surface loading (0.8 $\mu g\,cm^{-2}$) corresponds to a titania surface partially covered (estimated Au surface of 26.4 cm^2, leading to a surface coverage of less than 10%) by relatively small size metal particles. Further increase of the gold concentration results in metal particles of higher size which both reduce the available space on the semiconductor for pollutant adsorption and light absorption. Therefore, a significant decrease of the photocatalytic efficiency was observed at higher gold loadings.

4. Conclusions

Nanocrystalline titanium dioxide films developed on microscope glass slides were modified by gold deposition, characterized, and successfully tested for the photocatalytic degradation of the pollutant methyl orange. Titania photocatalysts with gold surface coverage of 0.8 $\mu g\,cm^{-2}$ were the most active and remained stable after several photocatalytic cycles of new added pollutant. The improvement in the photocatalytic efficiency of titania films by gold ions deposition is more than 100%. This enhancement is attributed to the action of Au particles, which play a key role by attracting conduction band photoelectrons and preventing electron-hole recombination.

Acknowledgments

We appreciate the valuable assistance from Dr. M.C. Bernard for obtaining the Raman spectra and from Stephan Borensztajn for taking the SEM images. Thanks are addressed to Delis AE Athens-Greece and Degussa AG Frankfurt-Germany for generously providing the TiO_2 Degussa P25 powder. Financial support from NATO (EST.CLG. 976641 grant) and GSRt/Ministry of Development/Greece (Excellence in the Research Institutes project) is also greatly acknowledged.

References

[1] A. Fujishima, T.N. Rao, D.A. Tryk, J. Photochem. Photobiol. C 1 (2000) 1.
[2] O.M. Alfano, D. Bahnemann, A.E. Cassano, R. Dillert, R. Goslich, Catal. Today 58 (2000) 199.
[3] A. Mills, S. Le Hunte, J. Photochem. Photobiol. A 108 (1997) 1.
[4] M. Miyauchi, A. Nakajima, T. Watanabe, K. Hashimoto, Chem. Mater. 14 (2002) 2812.
[5] E. Stathatos, P. Lianos, P. Falaras, A. Siokou, Langmuir 16 (2000) 2398.
[6] A. Fujishima, K. Hashimoto, T. Watanabe, TiO_2 Photocatalysis, Fundamentals and Applications, Bkc, Inc., Tokyo, 1999.
[7] N. Chandrasekharan, P.V. Kamat, J. Phys. Chem. B 104 (2000) 10851.
[8] V. Subramanian, E. Wolf, P.V. Kamat, J. Phys. Chem. B 105 (2001) 11439.
[9] M. Daté, Y. Ichihashi, T. Yamashita, A. Chiorino, F. Boccuzzi, M. Haruta, Catal. Today 72 (2002) 89.
[10] M. Valden, X. Lai, D.W. Goodman, Science 281 (1998) 1647.
[11] X.Z. Li, F.B. Li, Environ. Sci. Technol. 35 (2001) 2381.
[12] F. Boccuzzi, A. Chiorino, M. Manzoli, D. Andreeva, T. Tabakova, L. Ilieva, V. Idakiev, Catal. Today 75 (2002) 169.
[13] D. Andreeva, V. Idakiev, T. Tabakova, L. Ilieva, P. Falaras, A. Bourlinos, A. Travlos, Catal. Today 72 (2002) 51.
[14] M. Grätzel, R.F. Howe, J. Phys. Chem. 94 (1990) 2566.
[15] K.E. Karakitsou, X.E. Verykios, J. Phys. Chem. 97 (1993) 1184.
[16] I.M. Arabatzis, T. Stergiopoulos, M.C. Bernard, D. Labou, S.G. Neophytides, P. Falaras, Appl. Catal. B 42 (2003) 187.
[17] A. Dawson, P.V. Kamat, J. Phys. Chem. 105 (2001) 960.
[18] V. Subramanian, E.E. Wolf, P.V. Kamat, Langmuir 19 (2003) 469.
[19] D. Lahiri, V. Subramanian, T. Shibata, E.E. Wolf, B.A. Bunker, P.V. Kamat, J. Appl. Phys. 93 (2003) 2575.
[20] M. Haruta, Catal. Today 36 (1997) 153.
[21] Y.M. Gao, W. Lee, R. Trehan, R. Kershaw, K. Dwight, A. Wold, Mater. Res. Bull. 26 (1991) 1247.
[22] E. Bae, W. Choi, Environ. Sci. Technol. 37 (2003) 147.
[23] J. Lee, H. Park, W. Choi, Environ. Sci. Technol. 36 (2002) 5462.
[24] P.V. Kamat, M. Flumiani, A. Dawson, Colloids Surf. A 202 (2002) 269.
[25] A. Dodosz, A. Sobczynski, Monatsh. Chem. 132 (2001) 1045.
[26] F.B. Li, X.Z. Li, Appl. Catal. A 228 (2002) 15.
[27] I.M. Arabatzis, S. Antonaraki, T. Stergiopoulos, A. Hiskia, E. Papaconstantinou, M.C. Bernard, P. Falaras, J. Photochem. Photobiol. A 149 (2002) 237.
[28] E. Scolan, C. Sanchez, Chem. Mater. 10 (1998) 3217.
[29] I. Podolesheva, P. Gushterova, V. Platikanova, I. Konstantinov, J. Vac. Sci. Technol. A 16 (2) (1998) 674.
[30] A. Provata, P. Falaras, A. Xagas, Chem. Phys. Lett. 297 (1998) 484.
[31] C.J. Barbé, F. Arendse, P. Compte, M. Jirousek, F. Lenzmann, V. Shklover, M. Grätzel, J. Am. Ceram. Soc. 80 (1997) 3157.
[32] M.M. Alvarez, J.T. Khoury, T.G. Schaaff, M.N. Shafigullin, I. Vezmar, R.L. Whetten, J. Phys. Chem. B 101 (1997) 3706.
[33] P.V. Kamat, J. Phys. Chem. B 106 (2002) 7729.
[34] U. Kreibig, M. Gartz, A. Hilger, H. Hövel, in: E. Pelizzetti (Ed.), Fine Particles Science and Technology, Kluwer, Dordrecht, 1996, pp. 499–515.
[35] M.P. Seah, in: D. Briggs, M.P. Seah (Eds.), Practical Surface Analysis, Vol. 1, 2nd ed., Wiley, New York, 1990.
[36] A.P. Xagas, E. Androulaki, A. Hiskia, P. Falaras, Thin Solid Films 357 (1999) 173.
[37] T. Ioannides, X.E. Verykios, J. Catal. 161 (1996) 560.
[38] J. Nicole, D. Tsiplakides, C. Pliangos, X.E. Verykios, Ch. Comninellis, C.G. Vayenas, J. Catal. 204 (2001) 23.
[39] T. Uematsu, L. Fan, T. Maruyama, N. Ichikuni, S. Shimazu, J. Mol. Catal. A 182–183 (2002) 209.
[40] JCPDS Powder Diffraction File, Card 21-1272, JCPDS, International Centre for Diffraction Data, Swarthmore, PA, 1980.
[41] P. Falaras, A. Hugot-Le Goff, M.C. Bernard, A. Xagas, Sol. Energy Mater. Sol. Cells 64 (2000) 167.
[42] M. Ocana, V. Fornés, J.V. García-Ramos, C.J. Serna, J. Solid State Chem. 75 (1988) 364.
[43] J. Arbiol, J. Cerdà, G. Dezanneau, A. Cirera, F. Peiró, A. Cornet, J.R. Morante, J. Appl. Phys. 92 (2) (2002) 853.
[44] H. Al-Ekabi, N. Serpone, J. Phys. Chem. 92 (1988) 5726.
[45] N. Serpone, D. Lawless, R. Khairutdinov, E. Pelizzetti, J. Phys. Chem. 99 (1995) 16655.
[46] G. Katsaros, T. Stergiopoulos, I.M. Arabatzis, K.G. Papadokostaki, P. Falaras, J. Photochem. Photobiol. A 149 (2002) 191.
[47] P. Falaras, A.P. Xagas, J. Mater. Sci. 37 (2002) 3855.
[48] P. Falaras, I.M. Arabatzis, T. Stergiopoulos, M.C. Bernard, Int. J. Photoenergy 5 (2003) 123.
[49] C. Baiocchi, M.C. Brussino, E. Pramauro, A.B. Prevot, L. Palmisano, G. Marcì, Int. J. Mass Spectrometry 214 (2002) 247.
[50] Y. Nosaka, K. Norimatsu, H. Miyama, Chem. Phys. Lett. 106 (1984) 128.
[51] A. Sclafani, M.-N. Mozzanega, P. Pichat, J. Photochem. Photobiol. A 59 (1991) 181.